Electrochimica Acta 518 (2025) 145751

Contents lists available at ScienceDirect

Electrochimica Acta

journal homepage: www.journals.elsevier.com/electrochimica-acta

Impact of nitrogen functionalization and porosity on the electrosorption of ionic liquids on templated porous carbons

Zehui Guo [a], Marius Hermesdorf [a], Yongchao Chen [a], Ping Feng [a,b,c], Yan Lu [a,b,c], Martin Oschatz [a,b,d,*], Desirée Leistenschneider [a,d,*]

[a] Institute for Technical and Environmental Chemistry, Friedrich-Schiller University Jena, Philosophenweg 7a, 07743 Jena, Germany
[b] Helmholtz Institute for Polymers in Energy Applications Jena (HIPOLE Jena), Lessingstraße 12-14, 07743 Jena, Germany
[c] Institute of Electrochemical Energy Storage, Helmholtz-Zentrum Berlin für Materialien und Energie. 14109 Berlin, Germany
[d] Center for Energy and Environmental Chemistry Jena (CEEC Jena), Friedrich-Schiller University Jena, Philosophenweg 7a, 07743 Jena, Germany

ARTICLE INFO

Keywords:
Energy storage
Electric double-layer capacitor
Porous carbon
Nitrogen functionalization
Interfaces
Ionic liquids

ABSTRACT

This study systematically investigates the influence of nitrogen functionalities and their content in nitrogen-rich carbon materials, specifically carbon/carbon nitride nanohybrids, on their performance as electrode materials in electric double-layer capacitors (EDLCs) operated with ionic liquid electrolyte (1-Ethyl-3-methylimidazolium bis (trifluoromethylsulfonyl)imide). The loading amounts of cyanamide as carbon nitride precursor as well as the condensation temperature are varied over a wide range to obtain materials with significantly different porosity, nitrogen contents, and chemical properties of the nitrogen species. Thermogravimetric analysis, combustion elemental analysis, gas physisorption, and X-ray photoelectron spectroscopy measurements show that the nitrogen loss from carbon nitride starts to become significant between 500 and 600 °C and that different nitrogen species are created shifting from more pyridinic forms to graphitic and oxidized nitrogen. For the EDLC application, it is found that the mass-specific capacitance is dictated by the specific surface area whereas the capacitance normalized to the specific surface area determined by gas physisorption can be slightly enhanced by the presence of pyridinic nitrogen species. In addition, lowering of the total pore volume leads to higher areal active material loadings and lower dead volume which needs to be filled with electrolyte.

1. Introduction

As the global demand for clean and sustainable energy continues to rise, advanced energy storage technologies are critical to addressing the associated challenges [1,2]. Among these, electric double-layer capacitors (EDLCs), commonly also referred to as supercapacitors or ultracapacitors, have garnered considerable attention due to their ability to offer high power density, fast charge and discharge rates, and long cycle life [3–5]. EDLCs store energy through the formation of an electric double-layer at the interface between the electrode and the electrolyte. Ions are stored electrostatically and no chemical reactions take place neither in the electrodes nor in the electrolytes [6,7]. Due to this mechanism, they generally exhibit higher energy efficiencies at higher power densities in comparison to established battery systems. EDLCs are thus, utilized in certain applications with operating timescales in the range from milliseconds to seconds, particularly, in renewable energy systems and energy harvesting devices [8–10].

EDLC electrolytes can be categorized into solvent-based and solvent-free systems, with distinct behaviors in their properties and ion storage mechanisms [11,12]. In classical solvent-based electrolytes, such as inorganic or organic salts dissolved in either water or organic liquids, ions form a classical electric double-layer (EDL) at the electrified electrode surface. This EDL is characterized by the gradual accumulation of ions with opposite charge than the polarized surface under the increase of the electrode potential. As the surface becomes more and more charged, ions (as well as electrons or holes in the electrode) move closer together and form what is generally referred to as "compressed double-layer". The energy is thus, stored through increased proximity between the ions and the concentration gradient of ions depending on the distance to the electrode surface [4,13]. Moreover, in solvent-based electrolytes, bulk ions exist in the solvated state. Those solvation shells can be potentially removed when entering small nanometer-sized pores. Such phenomena can affect the final capacitance as well. On the one hand, due to decreased distances of ions and electrode surfaces, on

* Corresponding authors at: Institute for Technical and Environmental Chemistry, Friedrich-Schiller University Jena, Philosophenweg 7a, 07743 Jena, Germany.
E-mail addresses: martin.oschatz@uni-jena.de (M. Oschatz), desiree.leistenschneider@uni-jena.de (D. Leistenschneider).

https://doi.org/10.1016/j.electacta.2025.145751
Received 13 December 2024; Received in revised form 20 January 2025; Accepted 22 January 2025
Available online 23 January 2025

the other hand due to the energy demand needed for the removal of solvent molecules, which can lead to the storage of additional charges in the electrodes [14].

In contrast, the charge storage mechanism of solvent-free electrolytes, such as ionic liquids (ILs), cannot be described with the classical model of an electric double-layer based on Stern's theory [15]. The ionic building units of ILs interact via strong Coulombic forces, as well as H-bonds and are incompressible [16]. The presence of shells of solvate molecules can be ruled out in ILs, however, in their bulk state, ions are also characterized by a certain number of coordinating counterions, which can also be stripped off when entering pores with diameters in molecular dimensions [17,18]. Contrarily to solvent-based electrolytes, the number of free cations and anions is low due to their strong interactions with each other. Thus, different ionic arrangements formed on electrified interfaces have been proposed for solvent-free ILs, often associated with a change of their Coulombic ordering [19].

It is notable that at lower voltages, the energy storage is likely associated with single-ion inclusion in micropores, whereas at higher voltages, it is primarily governed by structural changes in the mesoscopic distance from the electrode surface. Here, in addition to the generally expected accumulation of similarly charged ions, other effects such as changes of the coordination number of the ions might contribute to energy storage as well [20,21]. Structural rearrangement may cause that the first adsorbed layer delivers a counter-ion charge exceeding that of the electrode surface. This is called "over-screening" [22]. To neutralize this excess charge, a second layer of ions with opposite polarity forms, and these oscillations extend and decay over several layers into the bulk [23,24]. The overall common sense is, that the interaction of ions within the bulk electrolyte in IL is strongly affecting the dissociation of ions and thus, the complete compensation of surface charge in case of increased polarization, either due to steric or coulombic effects. For the application of ILs in EDLCs, it therefore seems essential to establish specific interactions between the electrode and the electrolyte to densify the electric double-layer and thus, increase capacitance per electrode area [25–27]. Differently from solvent-based electrolytes, the strength of the direct ion adsorption by electrostatic, chemical or physical interaction can be expected to play a more important role for ILs. This, in turn, also provides an additional screw to regulate electrode-electrolyte interaction and local structures formed at this interface by strategies such as changing IL composition, electrode functionalization or addition of strongly adsorbing additives to the IL electrolytes [18,27,28].

Nitrogen functionalization of porous carbon electrodes can significantly improve the performance of IL-based supercapacitors [25,26,29]. In nitrogen-carbon materials, nitrogen atoms can be present in three major chemical bonding motives, namely graphitic, pyridinic, and pyrrolic [30]. Graphitic nitrogen thereby typically enhances the conductivity of carbon, while "pyridinic nitrogen" (typically used in literature as a summation of nitrogen in aromatic six-ring heterocycles, such as pyridine, triazine or pyrazine) facilitates electrode wetting and improved chemical interaction with ions due to the presence of electron-donating and electron-accepting binding sites [31,32]. One prominent example for such strongly adsorbing compounds are carbon nitride (C_3N_4) materials. Density functional theory (DFT) techniques have identified four possible sites for strong ion adsorption on carbon nitride electrodes, indicating their potential to densify the electric double-layer and further improve the performance of EDLCs [33]. However, in EDLC applications under relevant conditions, these sorption sites can only be utilized when the semiconducting carbon nitrides are combined with a conductive material. It seems challenging to combine strong ion binding and high electron conductivity simultaneously in a single phase of one nitrogen-containing carbon material. A promising strategy to minimize this problem is the formation of carbon/carbon nitride nanohybrids, which combine two different phases of nitrogen-functionalized carbon materials or a nitrogen-functionalized carbon and a pristine carbon material on the nm-scale [34,35].

When such nanohybrid materials (or also rather ordinary "nitrogen-doped carbon materials") are made, there is a complex interplay between porosity, chemical properties of the nitrogen species present, and their individual amounts and local distribution within the entire material. All these factors are influenced by the synthetic conditions and most often changing one synthetic parameter does change all these properties at the same time. Thus, the synthesis is expected to have a significant impact on the properties of the hybrid materials when applied as EDLC electrodes. Furthermore, in most cases, these relationships are investigated with relatively low nitrogen contents, typically below 10 wt.%. Consequently, there is a need for nitrogen-carbon materials which allow to discuss each single parameter by the rational design of a model sample matrix exhibiting different porosities, nitrogen functional groups and nitrogen contents. In the present study, a series of nitrogen-rich carbon/porous carbon nanohybrid materials is prepared in the temperature range from 500 to 800 °C. The use of different amounts of cyanamide as nitrogen precursor leads to nitrogen contents of ~1 to ~25 wt.% within a pristine carbon matrix. The synthesis-structure-property relationships of this series of model compounds, as well as of a physical mixture is then investigated in symmetrical EDLCs with 1-Ethyl-3-methylimidazolium bis(trifluoromethylsulfonyl)imide ionic liquid as the electrolyte. Thereby, this work elucidates the role of nitrogen functionalities and their amount as well as porosity for increasing the capacitance in IL based supercapacitors per area and volume.

2. Experimental

2.1. Synthesis of ZTC and NZTCs

Zinc oxide-templated carbon (ZTC) was prepared by employing ZnO as hard templates for well-defined mesopores (Scheme 1). 8 g ZnO nanoparticles (20–50 nm, provided by IBU-tec Advanced Materials AG, Weimar) were mixed with an aqueous solution consisting of 13 ml ultrapure water, 7 g sucrose (≥ 99.5 %, Sigma Aldrich) and 0.4 g NaOH (≥ 99 %, Carl Roth) in a Petri dish. Then the carbohydrate precursor underwent a poly-condensation at 100 °C for 3 h followed by subsequent heating to 160 °C for 6 h under air. Afterwards, the mixture was carbonized in a horizontal tubular furnace under N_2 flow. After purging the tube at 60 °C, a heating rate of 1 K min^{-1} was used from 60 °C to 950 °C. This temperature was held for 2 h under ~0.05 L min^{-1} nitrogen flow. A series of nitrogen-rich carbon/ZTC nanohybrid materials or an ordinary nitrogen-doped carbon material with varying nitrogen content and pore structures was then synthesized. This was achieved by adjusting the functionalization temperature and dispersing ZTCs in different amounts of aqueous cyanamide solution (99 %, Sigma Aldrich; 200 mg mL^{-1} prepared with ultrapure water). The mixture was dried in an oven at 60 °C, followed by cross-condensation at various temperatures for 4 h under ~0.05 L min^{-1} nitrogen flow with a heating rate of 1 K min^{-1} to yield the corresponding NZTCs (Scheme 1). NZTCs are further categorized into two groups: NDZTC, which stands for nitrogen-doped carbon, and CN-ZTC, which refers to ZTC/carbon nitride hybrid materials. The sample synthesized at the highest condensation temperature of 800 °C is designated as nitrogen-doped carbon (NDZTC). All ZTC/carbon nitride hybrid materials are labeled as CN-ZTCX Y:Z, where X denotes the condensation temperature in °C, and Y:Z indicates the mass ratio of ZTC: cyanamide.

2.2. Fabrication of supercapacitors

To prepare free-standing symmetrical electrodes for EDLCs, ZTCs/NZTCs, carbon black (C—NERGY Super C65, Nanografi Nano Technology), and polytetrafluoroethylene (PTFE, 60 wt.% solution in H_2O from Sigma Aldrich) were mixed with a mass ratio of ≈ 9:0.5:0.5 in a mortar and ground with ethanol repeatedly at a temperature around 100 °C until a film was formed. This film was then placed onto aluminum foil and hand-rolled to uniformly thin sheets (thicknesses 150 ± 10 μm) at

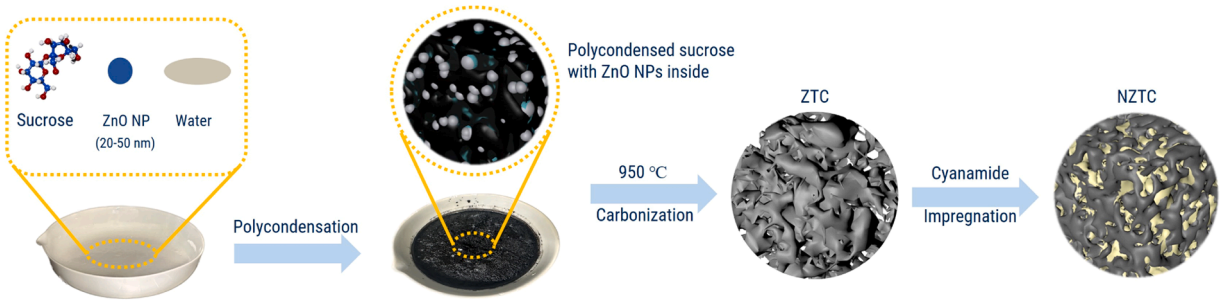

Scheme 1. Preparation of salt-templated carbons (ZTCs) and nitrogen-rich carbon/ZTC hybrid materials (NZTCs).

100 °C, followed by punching into free-standing electrode disks of 10 mm in diameter. The areal loadings of all electrodes were in the range of 2.8 - 5.3 mg cm^{-2} (**Table S1**). The electrodes were dried at 70 °C for 12 h under vacuum. EDLCs were tested in a symmetrical two-electrode configuration employing 1-Ethyl-3-methylimidazolium bis(trifluoromethylsulfonyl)imide (EMIMTFSI, ≥ 99.5 %, Sigma Aldrich) ionic liquid as the electrolyte. A Swagelok cell was assembled using a pair of circular electrodes sandwiching a separator (Whatman GF/D glass microfiber, 13 mm in diameter) with 150 µL electrolyte. The EDLCs with IL as electrolytes were assembled in an argon filled glove box (H_2O < 0.1 ppm, O_2 < 0.1 ppm).

2.3. Materials characterization

Thermogravimetric analyses (TGA) were performed on a Netzsch STA 449 in Al_2O_3 crucibles under N_2 in a temperature range from 25 °C to 1000 °C with a heating rate of 10 K min^{-1}. Argon physisorption measurements were carried out at −186 °C on a Vapor 200C Gassorption Analyzer from 3P Instruments. Prior to all measurements, the samples were degassed at 150 °C under vacuum for 24 h before each physisorption test. Quenched-solid density functional theory (QSDFT, for Ar at 87 K on carbon surfaces with cylindrical/sphere pores, adsorption branch kernel) was used for the calculation of the specific surface area and pore size distribution (PSD). Elemental analysis (EA) for carbon, hydrogen, and nitrogen (C/H/N) was conducted using a Vario Micro device through combustion analysis. X-Ray photoelectron spectroscopy (XPS) was conducted using a Thermo Scientific KAlpha spectrometer (monochromatic X-ray source: Al Kα anode 1486.6 eV). During analysis, pressure chamber was not exceeding 5×10^{-8} mbar. For charge compensation, a flood gun (NEK150-SC, Staib), which was calibrated to the C—C binding energy in polyethylene at 284.8 eV, was used. Survey scans to obtain the element composition were recorded with a step size of 1 eV and a pass energy of 100 eV For deconvolution of the nitrogen functional groups, high resolution spectra of C1 s, N1 s and O1 s were recorded as a sum of 5 individual scans. The step size of HR spectra was 0.05 eV and the pass energy was 30 eV The spot size for the measurement was 400 µm. Spectral fitting was done using the Avantage software (v 6.6.0).

The morphology of the obtained samples was analyzed using a JEOL-2100 transmission electron microscope (TEM) operated at an accelerating voltage of 200 kV. For TEM grid preparation, the samples were dispersed in 1 mL of ethanol and sonicated for 3 min to achieve a uniform dispersion. Subsequently, 15 µL of the dispersion was carefully deposited onto TEM grids (200-mesh copper grids with carbon support film, Electron Microscopy Sciences) and allowed to dry at room temperature under a fume hood.

2.4. Electrochemical measurements

To establish both nitrogen functionality and porosity-performance relationships of the NZTCs when applied in EDLCs, the NZTCs electrodes were characterized with cyclic voltammetry (CV) tests, galvanostatic charging/discharging with potential limitation (GCPL), as well as electrochemical impedance spectroscopy (EIS) in a frequency range from 100 kHz to 1 mHz with 6 frequencies per decade at 10 mV amplitude.

CV tests were performed at scan rates of 2–100 mV s^{-1}. The carbon differential gravimetric capacitance for CV plots, C_d (F g^{-1}) was calculated according to Eq. (1),

$$C_d = 2I/m\gamma \quad (1)$$

where I is the current (A), γ is the scan rate (V s^{-1}), and m is the active mass in one single carbon electrode (g).

GCPL was applied at specific currents between 0.1 and 10 A g^{-1} in a voltage range from 0 to +2.5 V. The carbon gravimetric capacitance, C (F g^{-1}), was calculated according to Eq. (2),

$$C = 2I\Delta t/\Delta Vm \quad (2)$$

where I (A) refers to the GCPL current, Δt (s) is the discharge time, m (g) represents the mass of the active material in a single electrode, and ΔV (V) corresponds to the discharge potential change within Δt excluding the IR drop.

3. Results and discussion

3.1. Influence of nitrogen functionalities

Thermogravimetric analysis of the ZTC material under air shows nearly complete combustion starting at ca. 400 °C (Fig. 1). Nitrogen-rich carbon was introduced into ZTC via an impregnation step using dicyanamide and a heat treatment at different temperatures. To monitor the mass changes during this heat treatment, TGA under nitrogen

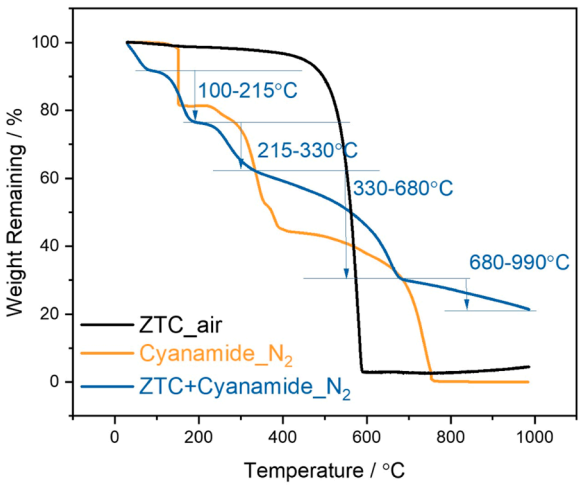

Fig. 1. TGA curves of pure cyanamide, pristine ZTC as well as ZTC-cyanamide mixture with mass ratio of 1:2.

atmosphere was utilized (Fig. 1). Cyanamide is well-known to undergo self-condensation. It starts forming carbon nitride at temperatures between 500 °C and 600 °C [36,37]. The resulting carbon nitride then becomes unstable around 600 °C, and decomposes into small nitrogen-containing species, such as ammonia and gaseous cyano fragments [38]. This can also be seen in the TGA profile of ZTC infiltrated with cyanamide. The first two mass loss steps can be assigned to evaporation of volatile species, which may stem from residual solvent or water. Subsequently, additional mass losses can be seen at 215 - 330 °C, and 330 - 680 °C, which mainly correspond to the polycondensation and formation of carbon nitride. Lastly, the mass loss above 680 °C is assigned to the conversion of carbon nitride to N-doped carbon. Consequently, 800 °C, 650 °C, 600 °C, and 500 °C were selected as functionalization temperatures for nitrogen-rich carbons (NZTCs) to obtain materials with varying nitrogen functionalities and contents. TGA measurements also indicate that the cyanamide is really infiltrated and confined into the ZTC matrix prior to condensation as the mass profile is shifted and changed in shape as compared to the pristine cyanamide. According to the TGA and elemental analysis results, the sample functionalized at 800 °C is nitrogen-doped carbon (NDZTC), while the others are carbon / carbon nitride composites (CN-ZTC). The nitrogen content of NDZTC is as low as 0.97 wt.%. In contrast, CN-ZTC650, CN-ZTC600, and CN-ZTC500 have nitrogen contents of 1.71 wt.%, 3.56 wt.%, and 24.84 wt.%, respectively, as detected by elemental analysis (Table 1). The survey XPS spectra of ZTC, NDZTC, and CN-ZTC samples show the presence of carbon, nitrogen, and oxygen (Fig. 2**a**). Analysis of the elemental contents (**Table S2**) confirms the increase of nitrogen content with decreasing functionalization temperature.

XPS was employed to characterize and specify the chemical structure of the nitrogen-containing functional groups [39]. A trace of 2.7 wt.% residual zinc is detected in ZTC but there is no metal content in the NZTC materials. Deconvolution of the high-resolution N 1 s spectra (Fig. 2**b-e**) of CN-ZTC500, CN-ZTC600, and CN-ZTC650 further reveal five peaks representing nitrogen with a similar chemical environment such as pyridinic nitrogen (398.5 eV), pyrrolic nitrogen (400.1 eV), graphitic nitrogen (401.2 eV), oxidized nitrogen (402.6 eV) [28,40,41], and nitrite (NO_2^-) nitrogen (404.5 eV) [42] but with varying relative contents of these nitrogen species. It is noteworthy that the deconvolution of the N1 s spectrum of NDZTC is difficult due to the high signal-to-noise ratio. The presence of nitroxides (404.5 eV) cannot be determined in this sample.

As the temperature increases from 500 °C to 800 °C, the relative proportion of pyridinic nitrogen in NZTCs decreases, while the amounts of pyrrolic nitrogen and graphitic nitrogen increase. This trend is clearly reflected in the ratio of pyridinic nitrogen to pyrrolic nitrogen, which is 2.6 for CN-ZTC500, 1.5 for CN-ZTC600, 1.4 for CN-ZTC650, and 0.9 for NDZTC. These results underline that nitrogen in CN-ZTC500 is predominantly present as pyridinic nitrogen.

Table 1
Mass ratio of ZTC to cyanamide, DFT specific surface area (SSA), DFT total pore volume (V_t), as well as the nitrogen content of NDZTC and CN-ZTC samples.

Sample	ZTC: Cyanamide (weight)	DFT		N amount (wt.%)
		SSA (m^2 g^{-1})	V_t (cm^3 g^{-1})	
ZTC	1:0	1362	1.17	-
NDZTC	1:2	1233	0.87	0.97
CN-ZTC650	1:2	1416	1.06	1.71
CN-ZTC600	1:2	1346	0.99	3.56
CN-ZTC500	1:2	165	0.16	24.84
CN-ZTC500 1:1	1:1	450	0.49	17.78
CN-ZTC500 1:0.5	1:0.5	862	0.72	10.81
CN-ZTC500 1:1 P	1:1	962	0.74	15.82

Note: CN-ZTC500 1:1 P refers to the physical mixture of ZTC and carbon nitride derived from cyanamide at 500 °C for 4 h under a 0.005 L/min nitrogen flow, mixed in a 1:1 mass ratio with ZTC and cyanamide.

ZTC shows a type IV isotherms in argon physisorption [43] with H3 hysteresis loop at a relative pressure ranging from 0.40 to 0.99, indicating a multimodal porosity including micro- and mesopores (Fig. 3; Table 1). In contrast, NDZTC, CN-ZTC650, and CN-ZTC500 exhibit type I isotherms, whereas CN-ZTC600 presents a type II isotherm, implying that some mesopores are blocked by carbon nitride. Among the nitrogen-rich samples, CN-ZTC500 displays notably lower argon uptake, suggesting that the ZTC micropores were widely blocked by carbon nitride.

The electrochemical performance of pure EMIMTFSI IL as electrolyte, paired with ZTC / NDZTC / CN-ZTC electrodes, was investigated in a free-standing symmetrical two-electrode configuration. First of all, it can be seen that in tendency a higher mass of samples with lower porosity can be loaded per electrode area at comparable thickness (**Table S1**). Achieving a high areal loading is important for a high practical energy density of EDLCs on cell level. In addition, less electrolyte which does itself not contribute to capacitance needs to be added if the electrode materials are less porous. Electrochemical impedance spectroscopy (EIS) has been used to characterize resistive behavior of the electrodes [44,45]. According to the physicochemical transport model proposed by Mei et al., the low-frequency region reflects the diffuse layer resistance, while the intermediate-frequency region corresponds to the electrolyte resistance. The high-frequency region represents the electrode resistance, and the combined resistance of the electrode and electrolyte according to the proposed model. This internal resistance showed good agreement with the internal resistance derived from the IR drop observed in GCPL measurements [44]. All Nyquist plots display an almost vertical orientation in the low-frequency region beginning at around 0.15 Hz (Fig. 4**a**), indicative of capacitive behavior. ZTC demonstrates the lowest internal resistance, yet, shows the highest diffuse layer resistance. This outcome can be attributed to the nitrogen species, which, while reducing the electrode's conductivity, enhances the equilibration of ion binding to the electrode surface, by decreasing diffuse layer resistance. The CV curves show nearly rectangular shapes from 0 to 2.5 V at various scan rates (Fig. 4**b; Fig. S1**), the GCPL curves are close to symmetrical triangle at a low current density of 0.1 A g^{-1} (Fig. 4**d**), which is a typical characteristic of an ideal electric double-layer capacitor behavior. Under the conditions of the measurements, none of the nitrogen-carbon compounds seems to induce contributions of Faradaic processes. CN-ZTC500 has the smallest integral CV area and largest IR drop in the GCPL curve, indicating the largest internal resistance due to the restricted accessibility of the electrode surface after blocking of the microporous structure, with a large portion of the carbon surface not being accessible even during a slow, quasi-equilibrium charging / discharging process. At a low current density of 0.1 A g^{-1}, the specific capacitance of ZTC reaches 117 F g^{-1} (Fig. 4**c**). With the decrease of the functionalization temperature, the mass-specific capacitance decreases from 107 F g^{-1} (NDZTC) to 17 F g^{-1} (CN-ZTC500). This is, first of all, mainly related to the lower specific surface area (Table 1).

Capacitance is closely related to the specific surface area of electrodes. The polarity, however, which depends on the functionality of nitrogen can influence the wettability due to the specific interactions between IL ions and accessible adsorption sites in the carbon pore walls and thus, the capacitance as well. Therefore, capacitance have been normalized to the specific surface area determined by argon physisorption. At 0.1 A g^{-1}, the normalized specific capacitances are 0.086 F m^{-2} (ZTC), 0.087 F m^{-2} (NDZTC), 0.066 F m^{-2} (CN-ZTC650), 0.077 F m^{-2} (CN-ZTC600), and 0.104 F m^{-2} (CN-ZTC500) (Fig. 4e,f). CN-ZTC500 has the largest area-normalized area in CV curve, and the highest normalized capacitance retention. To evaluate the influence of surface area and nitrogen content on capacitance, plots of surface area and nitrogen content versus capacitance were generated (**Fig. S2**). The results reveal that capacitance is affected not only by surface area, but also

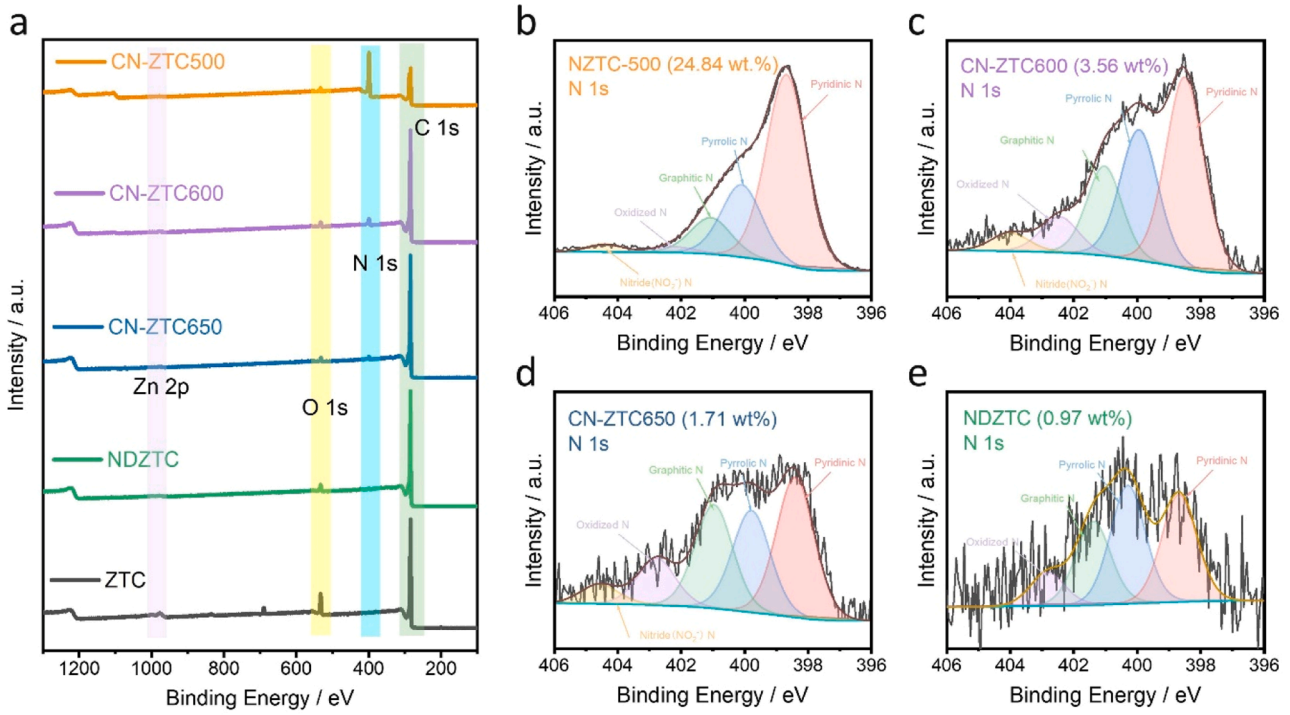

Fig. 2. a) XPS survey spectra (spectrum of ZTC is shown for comparison) and b-e) fitted high-resolution XPS N1 s spectra of CN-ZTC500, CN-ZTC600, NC-ZTC650, and NDZTC.

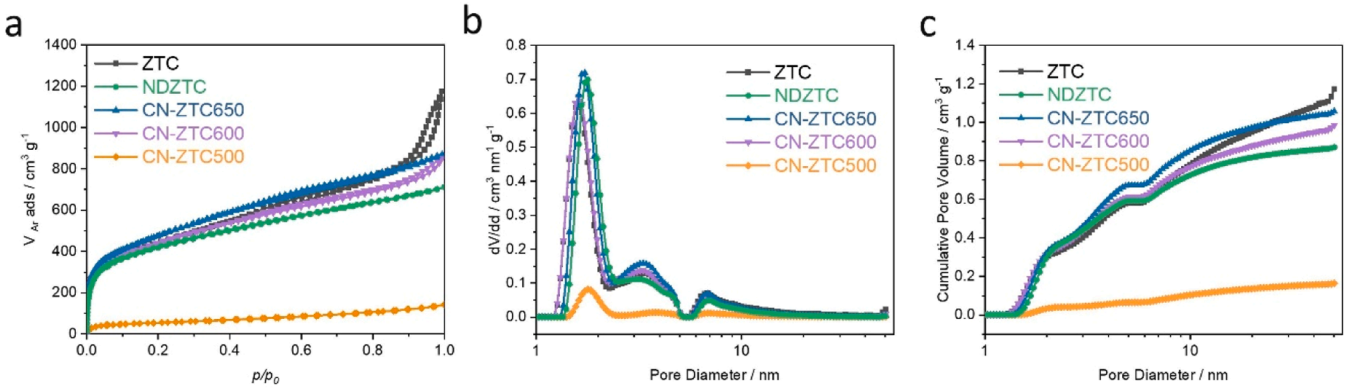

Fig. 3. a) Argon physisorption isotherms measured at 87 K; b) differential plots of pore size distributions calculated from QSDFT model, adsorption branch kernel; c) cumulative pore size distribution plots of ZTC, NDZTC, and CN-ZTC samples synthesized at different temperature.

significantly depends on nitrogen content.

3.2. *Influence of nitrogen content*

A comparable content of (particularly pyridinic) nitrogen in NDZTC and CN-ZTC samples cannot be obtained by changing the functionalization temperature, as it will also change the ratio of N-containing groups as could be seen via XPS (Fig. 2). Therefore, the ratio was adjusted by varying the mass-ratio of ZTC to cyanamide from 1:2 to 1:1 and 1:0.5 at the constant condensation temperature of 500 °C. Argon physisorption isotherms (Fig. 5) reveal that CN-ZTC500 1:0.5 and CN-ZTC500 1:1 have additional mesopores and increased porosity compared to CN-ZTC500 1:2.

TEM images (Fig. 6**a**) reveal that ZTC possesses an open morphology with a nanostructure including mesopores, which is maintained even after functionalization in CN-ZTC500 1:0.5 and CN-ZTC500 1:1 (Fig. 6**b, c**). However, CN-ZTC500 1:2 (Fig. 6**d**) exhibits a nearly closed pore nanostructure. This effect is attributed to the substantial presence of stacked carbon nitride sheets (Fig. 6**h**) which do not have an intrinsic porosity, consistent with the argon physisorption result. As the cyanamide ratio increases from 1:0.5 to 1:2, CN-ZTC500 samples demonstrate progressively larger areas of stacked layers (Fig. 6**f-h**), due to the more pronounced contribution of carbon nitride with increasing stacking height from CN-ZTC500 1:0.5 to CN-ZTC500 1:2. This adjustment achieved nitrogen contents of 10.81 wt.% for CN-ZTC500 1:0.5, 17.78 wt.% for CN-ZTC500 1:1, and 24.84 wt.% for CN-ZTC500 1:2 (Table 1). The N1 s XPS fitting results indicate that CN-ZTC500 1:0.5, CN-ZTC500 1:1, and CN-ZTC500 1:2 exhibit a comparable distribution of nitrogen species (Fig. 7). All samples are characterized by the dominant presence of pyridinic nitrogen, with smaller amounts of pyrrolic nitrogen, and even lower proportions of graphitic nitrogen. Additionally, there are minor contributions from oxidized nitrogen and nitride nitrogen. Thus, CN-ZTC500 samples allow for the investigation of the absolute nitrogen content on the capacitance and the electric conductivity, without an

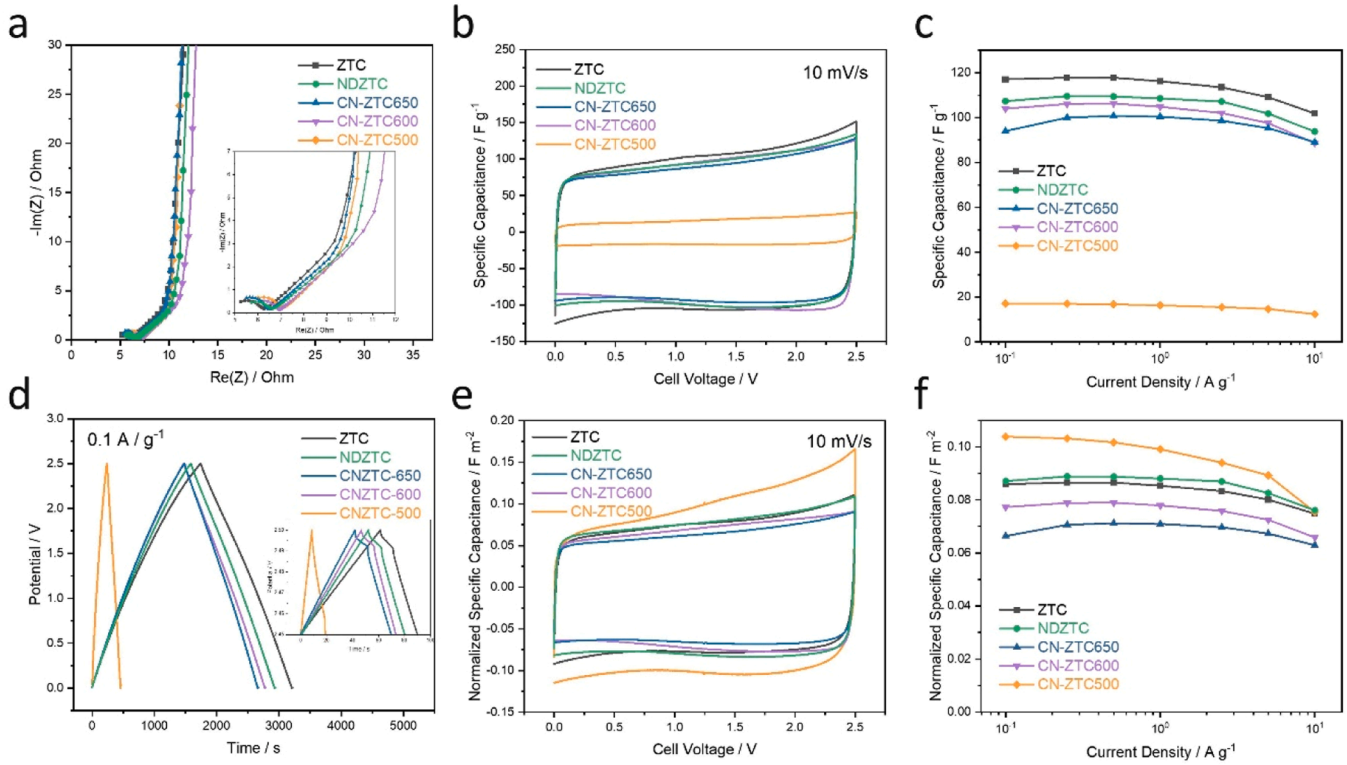

Fig. 4. EDLC performance of the ZTC, NDZTC, CN-ZTC650, CN-ZTC600, and CN-ZTC500 tested in EMIMTFSI ionic liquid electrolyte using a two-electrode configuration: a) Nyquist plots with a zoomed-in view of intermediate-frequency region; b) cyclic voltammograms at 10 mV s^{-1}; c) capacitance retention with current density increase; d) galvanostatic charging / discharging with potential limitation at 0.1 A g^{-1} with a zoom into the IR region in the inset; e-f) cyclic voltammograms at 10 mV s^{-1} and capacitance retention with current density increase, both normalized by specific surface area.

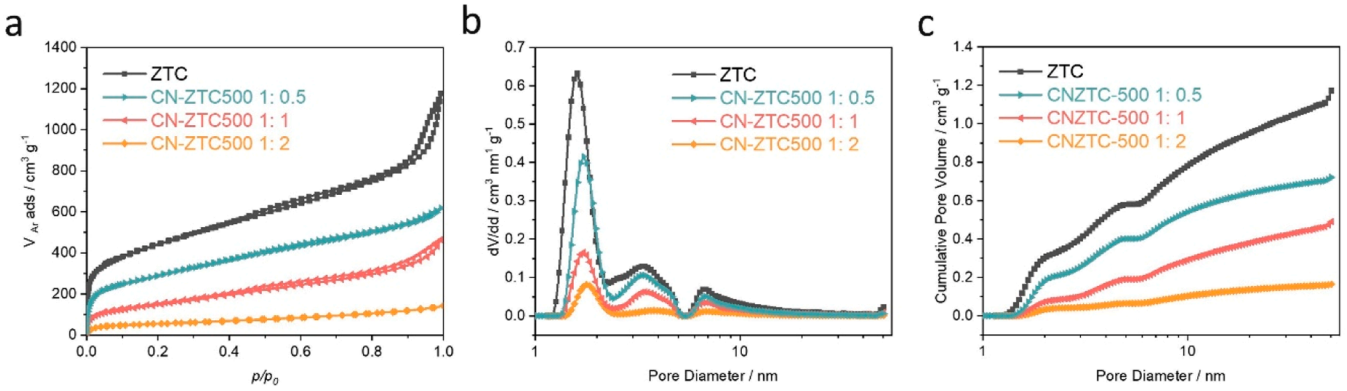

Fig. 5. a) Argon physisorption isotherms measured at 87 K of ZTC, CN-ZTC500 1:0.5, CN-ZTC500 1:1, and CN-ZTC500 1:2; b) differential plots of pore size distributions calculated from QSDFT model, adsorption branch kernel; c) cumulative pore size distribution plots.

overlapping influence of a different surface chemistry.

The electrochemical performance of CN-ZTC500 electrodes were again assessed in free-standing symmetrical two-electrode Swagelok cell configurations. As well as for the temperature series discussed before, electrode areal loadings increase with increasing content of carbon nitride. The Nyquist plots exhibit a consistent profile among the CN-ZTC electrodes, characterized by an almost vertical curve progression in the low-frequency domain (Fig. 8**a**). CN-ZTC500 1:0.5 and ZTC reveal nearly identical internal resistance, both of which are lower than those of CN-ZTC500 1:1 and CN-ZTC500 1:2 in Nyquist plot. Nevertheless, CN-ZTC500 devices demonstrate lower diffuse layer resistance than the ZTC device, indicating that, as the carbon nitride content increases, polarization and electric formation of the IL/carbon interface within CN-ZTC500 devices equilibrates more rapidly. The cyclic voltammetry (CV) curves again demonstrate nearly rectangular shapes within the voltage range of 0 to 2.5 V at various scan rates (Fig. 8**b; Fig. S3**). All CN-ZTC500 samples exhibit a lower capacitance than ZTC (Fig. 8**c**). The GCPL profiles exhibit a nearly symmetrical triangular shape at a low current density of 0.1 A g^{-1} (Fig. 8**d**), indicating efficient charge-discharge characteristics. At this current density, the measured IR drop values are 6.8 Ω for ZTC, 7.0 Ω for CN-ZTC500 1:0.5, 8.0 Ω for CN-ZTC500 1:1, and a substantially higher 64.2 Ω for CN-ZTC500 1:2. These results suggest that samples with lower carbon nitride content display higher conductivity, consistent with the typical behavior of electric double-layer capacitors. Additionally, at this current density, the CN-ZTC500 1:0.5 achieves a specific capacitance of 54 F g^{-1}, as determined through GCPL measurements (Fig. 8**c**). Conversely, with the incremental addition of carbon nitride, the specific capacitance declines to

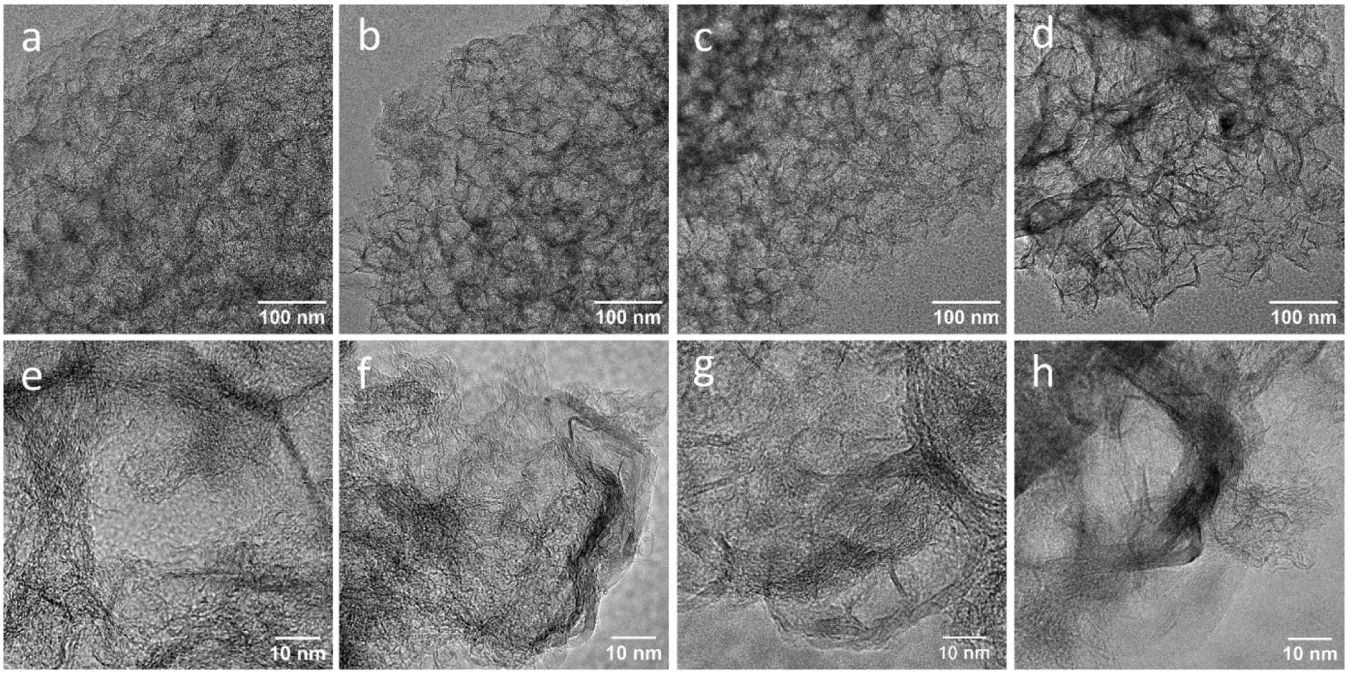

Fig. 6. TEM images of a, e) ZTC; b, f) CN-ZTC500 1:0.5; c, g) CN-ZTC500 1:1; and d, h) CN-ZTC500 1:2.

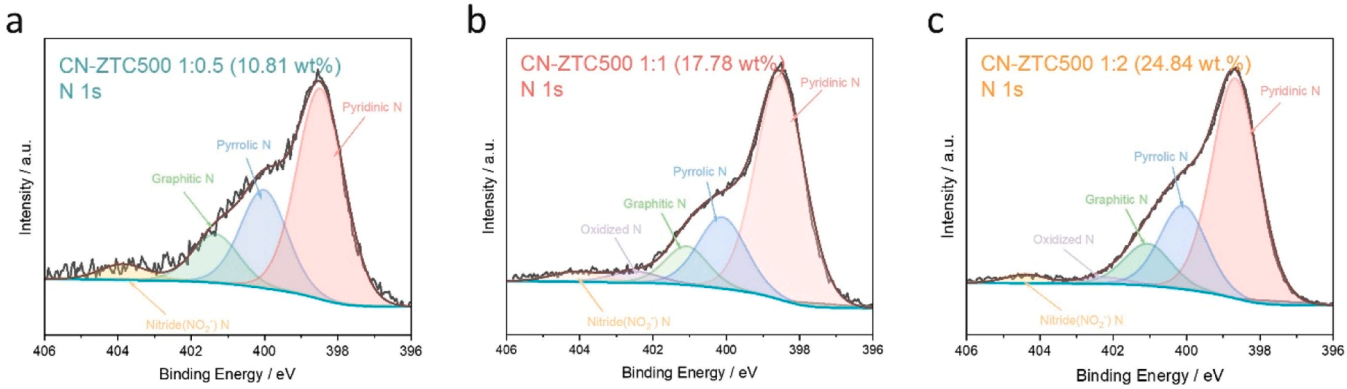

Fig. 7. Fitted high-resolution XPS N1 s spectra of CN-ZTC500 1:0.5, CN-ZTC500 1:1, and CN-ZTC500 1:2, respectively.

38 F g^{-1} for CN-ZTC500 1:1, eventually reaching 17 F g^{-1} for CN-ZTC500 1:2, which correlates with a reduction in specific surface area values (Table 1, **Fig. S4a**). Both the specific capacitance and capacitance retention, normalized to the DFT-derived SSA of the electrodes, were employed to assess the influence of nitrogen content (Fig. 8**e, f**). Notably, CN-ZTC500 1:2 continues to exhibit the largest normalized integrated area in the CV curve and the highest normalized capacitance retention, attributable to its elevated proportion of nitrogen (**Fig. S4b**).

To evaluate the electrochemical performance of a carbon/carbon nitride nanohybrid material compared to a carbon/carbon nitride physical mixture, CN-ZTC500 1:1 and its physical mixture counterpart, CN-ZTC500 1:1 P were selected, along with pure carbon nitride synthesized from cyanamide and carbonized under identical conditions as used for the functionalization. The nitrogen contents of CN-ZTC500 1:1 and CN-ZTC500 1:1 P as determined from elemental analysis are in the same range (Table 1). Argon physisorption isotherms reveal that carbon nitride contains no nitrogen-detectable porosity at all, while CN-ZTC500 1:1 and CN-ZTC500 1:1 P exhibit both micropores and mesopores. Notably, the pore volume and SSA of CN-ZTC500 1:1 lie between those of the physical mixture (CN-ZTC500 1:1 P) and pure carbon nitride (**Fig. S5,** Table 1). Given the comparable nitrogen content in both samples, this confirms that the carbon nitride phase is indeed located within the pore system of ZTC in case of the CN-ZTC500 1:1 nanohybrid material. The CV and GCPL results show that the capacitance of CN-ZTC500 1:1 corresponds to 57 % of that of the CN-ZTC500 1:1 physical mixture (**Fig. S6**). This is in line with the lower pore volume and SSA of the nanohybrid material. The CV results of pure carbon nitride indicate a marginal capacitance of only 0.04 F g^{-1}, as calculated from GCPL at a current density of 0.1 A g^{-1}. That means the capacitance of the CN-ZTC500 1:1 physical mixture electrode is entirely originating from ZTC. For the example of the nanohybrid material discussed here, the obtained specific capacitance of the physical mixture is in good accordance with the mass ratio of ZTC:carbon nitride which is roughly 3:1. In the nanohybrid material, the capacitance is decreased even further because a certain portion of the porosity of ZTC is blocked in addition to the contribution of the mass of carbon nitride. Notably, the electrode mass loading decreases with the increasing carbon nitride content, from 4.7 mg cm^{-2} for CN-ZTC500 1:2 to 4.0 mg cm^{-2} for CN-ZTC500 1:1 and 3.1 mg cm^{-2} for CN-ZTC500 1:0.5 (**Table S1**).

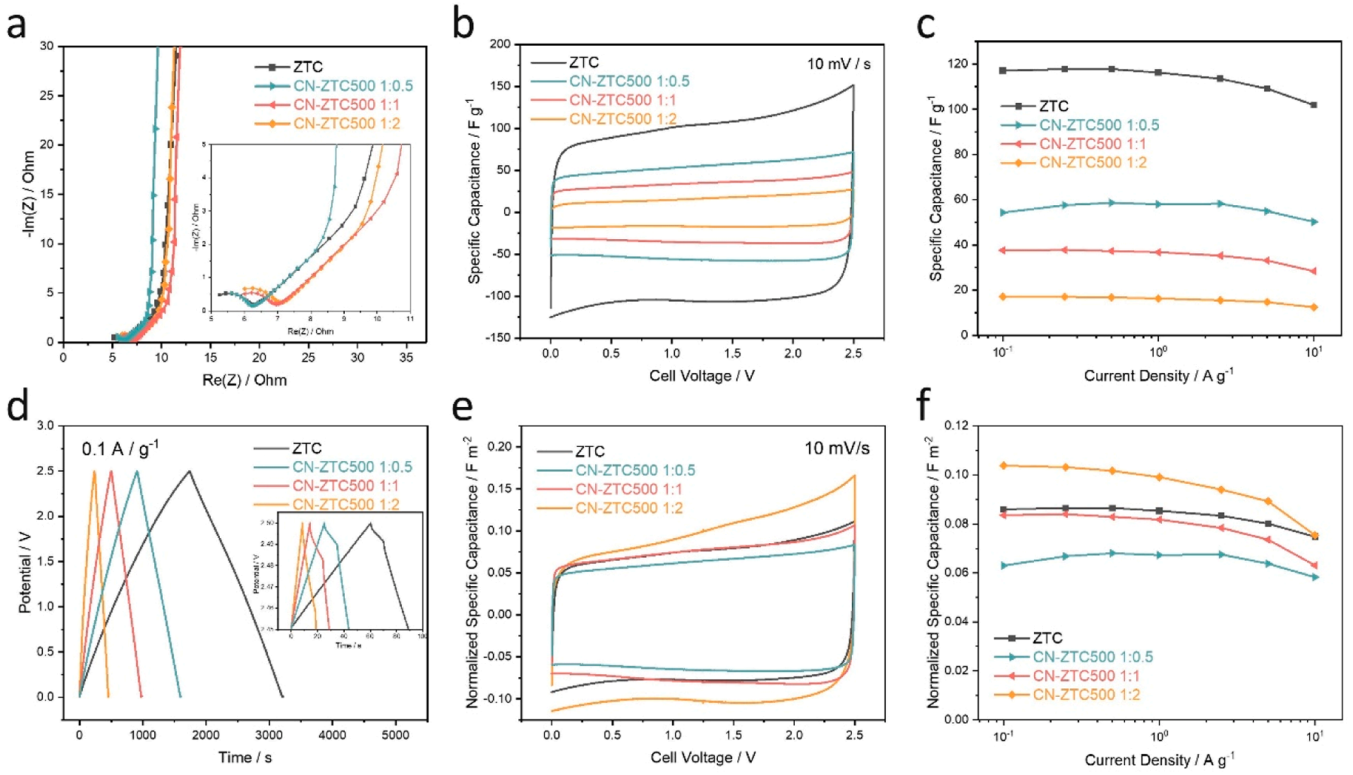

Fig. 8. EDLC performance of the ZTC, CN-ZTC500 1:0.5, CN-ZTC500 1:1, and CN-ZTC500 1:2 tested in EMIMTFSI ionic liquid electrolyte using a two-electrode configuration: a) Nyquist plots with a zoomed-in view of intermediate-frequency region; b) cyclic voltammograms at 10 mV s^{-1}; c) capacitance retention with current density increase; d) galvanostatic charging / discharging with potential limitation at 0.1 A g^{-1}, including a zoom of IR region; e-f) cyclic voltammograms at 10 mV s^{-1} and capacitance retention with current density increase, both normalized by specific surface area.

4. Conclusion

A porous carbon material with large mesopores obtained by using ZnO nanoparticles of 20 - 50 nm as template has been used as a model matrix to investigate the effect of different nitrogen loading amounts, different nitrogen species, and different remaining porosity on the properties of IL-based EDLCs. On the one hand, it has been shown that cyanamide condensation at temperatures between 500 and 800 °C leads to a gradual decrease of the nitrogen content, change of the chemical bonding motives of the nitrogen species from pyridinic to graphitic and oxidized forms and to a gradual increase in porosity. The chemical properties of the nitrogen species present expectedly depend on the condensation temperature. In addition, a series of samples with different content of pyridinic nitrogen has been prepared by changing the cyanamide loading at constant condensation temperature of 500 °C. It is found that, while the mass-specific capacitance is dictated by the specific surface area, the area-normalized capacitance can be slightly enhanced by the presence of pyridinic nitrogen species. In addition, lowering of the total pore volume leads to higher areal active material loadings and lower dead volume, which needs to be filled with electrolyte, which is in case of IL supercapacitors a relevant cost factor. Comparison between the formed nanohybrids and a purely physical mixture between ZTC and carbon nitride shows that the chosen infiltration-condensation method indeed leads to the formation of carbon nitride within the pore system of ZTCs. All in all, our study provides a systematic investigation about the synthesis-structure-property-relationships of nitrogen-functionalized carbon materials as EDLC electrodes and gives insights into the interplay between nitrogen content, nitrogen species, and porosity on the properties of the materials when applied as electrodes in EDLCs.

CRediT authorship contribution statement

Zehui Guo: Writing – original draft, Investigation, Data curation, Conceptualization. **Marius Hermesdorf:** Investigation. **Yongchao Chen:** Investigation. **Ping Feng:** Investigation. **Yan Lu:** Investigation. **Martin Oschatz:** Writing – review & editing, Supervision, Project administration, Funding acquisition. **Desirée Leistenschneider:** Writing – review & editing, Supervision, Project administration, Funding acquisition.

Declaration of competing interest

The authors declare the following financial interests/personal relationships which may be considered as potential competing interests:

Zehui Guo reports financial support was provided by China Scholarship Council. Desiree Leistenschneider reports financial support was provided by Carl-Zeiss Foundation. Martin Oschatz reports financial support was provided by European Research Council. Yongchao Chen reports financial support was provided by federal state of Thuringia und ESF plus. Marius Hermesdorf reports financial support was provided by Fonds der Chemischen Industrie. If there are other authors, they declare that they have no known competing financial interests or personal relationships that could have appeared to influence the work reported in this paper.

Acknowledgment

Z.G. acknowledges financial support from China Scholarship Council (CSC). M.O. acknowledges funding by the European Union (ERC, CIL-Cat, project number 101040394). The views and opinions presented are solely those of the author(s) and do not necessarily represent those of the European Union or the European Research Council Executive Agency.

The European Union and the granting authority are not liable for any statements made. Part of this research has also been financially supported by the Research Unit DeKarbon – *Selective Deposition and Chemical Conversion of Carbon Dioxide on Nanostructured Polymer Materials* (FTI Thüringen PERSONEN, 2022 FGR 0001), supported by the Free State of Thuringia and the European Social Fund Plus. M. H. and D. L. acknowledge the Fonds der Chemischen Industrie for financial support through the Liebig fellowship. D. L. thanks the Carl-Zeiss-Stiftung for financial support of the project ReAlBatt within the Nexus program.

Supplementary materials

Supplementary material associated with this article can be found, in the online version, at doi:10.1016/j.electacta.2025.145751.

Data availability

Data will be made available by the corresponding authors upon reasonable request.

References

[1] P. Simon, Y. Gogotsi, Capacitive energy storage in nanostructured carbon–electrolyte systems, Acc. Chem. Res. 46 (2013) 1094–1103, https://doi.org/10.1021/ar200306b.
[2] M. Kaur, P. Chand, H. Anand, Aarti, Fabrication of asymmetric supercapacitor device with $NiCo_2O_4$@ reduced graphene oxide nanocomposites, Electrochim. Acta 507 (2024) 145118, https://doi.org/10.1016/j.electacta.2024.145118.
[3] P. Simon, Y. Gogotsi, Perspectives for electrochemical capacitors and related devices, Nat Mater 19 (2020) 1151–1163, https://doi.org/10.1038/s41563-020-0747-z.
[4] F. Béguin, V. Presser, A. Balducci, E. Frackowiak, Carbons and electrolytes for advanced supercapacitors, Adv. Mater. 26 (2014) 2219–2251, https://doi.org/10.1002/adma.201304137.
[5] X. Chen, R. Paul, L. Dai, Carbon-based supercapacitors for efficient energy storage, Natl Sci Rev 4 (2017) 453–489, https://doi.org/10.1093/nsr/nwx009.
[6] P. Simon, Y. Gogotsi, B. Dunn, Where do batteries end and supercapacitors begin? Science 343 (2014) 1210–1211, https://doi.org/10.1126/science.1249625.
[7] S. Fleischmann, Y. Zhang, X. Wang, P.T. Cummings, J. Wu, P. Simon, V. Augustyn, Continuous transition from double-layer to faradaic charge storage in confined electrolytes, Nature Energy 7 (2022) 222–228, https://doi.org/10.1038/s41560-022-00993-z.
[8] J. Libich, J. Máca, J. Vondrák, O. Čech, M. Sedlaříková, Supercapacitors: properties and applications, J. Energy Storage 17 (2018) 224–227, https://doi.org/10.1016/j.est.2018.03.012.
[9] K. Dissanayake, D. Kularatna-Abeywardana, A review of supercapacitors: materials, technology, challenges, and renewable energy applications, J. Energy Storage 96 (2024) 112563, https://doi.org/10.1016/j.est.2024.112563.
[10] X. Pan, F. Ji, Q. Xia, X. Chen, H. Pan, S.N. Khisro, Y. Zhang, High-performance supercapacitors based on superior Co3O4 nanorods electrode for integrated energy harvesting-storage system, Electrochim. Acta 282 (2018) 905–912, https://doi.org/10.1016/j.electacta.2018.06.127.
[11] L. Nègre, B. Daffos, P.-L. Taberna, P. Simon, Solvent-free electrolytes for electrical double layer capacitors, J Electrochem Soc 162 (2015) A5037, https://doi.org/10.1149/2.0061505jes.
[12] C. Wolff, S. Jeong, E. Paillard, A. Balducci, S. Passerini, High power, solvent-free electrochemical double layer capacitors based on pyrrolidinium dicyanamide ionic liquids, J Power Sources 293 (2015) 65–70, https://doi.org/10.1016/j.jpowsour.2015.05.065.
[13] C. Zhong, Y. Deng, W. Hu, J. Qiao, L. Zhang, J. Zhang, A review of electrolyte materials and compositions for electrochemical supercapacitors, Chem Soc Rev 44 (2015) 7484–7539, https://doi.org/10.1039/C5CS00303B.
[14] J. Chmiola, G. Yushin, Y. Gogotsi, C. Portet, P. Simon, P.L. Taberna, Anomalous increase in carbon capacitance at pore sizes <1 nanometer, Science 313 (2006) 1760–1763, https://doi.org/10.1126/science.1132195.
[15] A. Kumar, G. Ahmed, M. Gupta, P. Bocchetta, R. Adalati, R. Chandra, Y. Kumar, Theories and models of supercapacitors with recent advancements: impact and interpretations, Nano Express 2 (2021) 022004, https://doi.org/10.1088/2632-959X/abf8c2.
[16] D.H. Zaitsau, V.N. Emel'yanenko, P. Stange, S.P. Verevkin, R. Ludwig, Dissecting the vaporization enthalpies of ionic liquids by exclusively experimental methods: coulomb interaction, hydrogen bonding, and dispersion forces, Angew. Chemie Int. Ed. 58 (2019) 8589–8592, https://doi.org/10.1002/anie.201904813.
[17] C. Largeot, C. Portet, J. Chmiola, P.L. Taberna, Y. Gogotsi, P. Simon, Relation between the ion size and pore size for an electric double-layer capacitor, J. Am. Chem. Soc. 130 (2008) 2730–2731, https://doi.org/10.1021/ja7106178.
[18] R. Yan, M. Antonietti, M. Oschatz, Toward the experimental understanding of the energy storage mechanism and ion dynamics in ionic liquid based supercapacitors, Adv Energy Mater 8 (2018) 1800026, https://doi.org/10.1002/aenm.201800026.
[19] R. Futamura, T. Iiyama, Y. Takasaki, Y. Gogotsi, M.J. Biggs, M. Salanne, K. Kaneko, Partial breaking of the coulombic ordering of ionic liquids confined in carbon nanopores, Nat Mater 16 (2017) 1225–1232, https://doi.org/10.1038/nmat4974.
[20] M. Antonietti, X. Chen, R. Yan, M. Oschatz, Storing electricity as chemical energy: beyond traditional electrochemistry and double-layer compression, Energy Environ Sci 11 (2018) 3069–3074, https://doi.org/10.1039/C8EE01723A.
[21] K. Schutjajew, R. Yan, M. Antonietti, C. Roth, M. Oschatz, Effects of carbon pore size on the contribution of ionic liquid electrolyte phase transitions to energy storage in supercapacitors, Front. Mater. 6 (2019) 65, https://doi.org/10.3389/fmats.2019.00065.
[22] F. Bresme, O. Robotham, W.-I.K. Chio, M.A. Gonzalez, A. Kornyshev, Debye screening, overscreening and specific adsorption in solutions of organic ions, Physical Chemistry Chemical Physics 20 (2018) 27684–27693, https://doi.org/10.1039/C8CP04924F.
[23] V. Ivaništšev, K. Kirchner, T. Kirchner, M.V. Fedorov, Restructuring of the electrical double layer in ionic liquids upon charging, Journal of Physics: condensed matter 27 (2015) 102101, https://doi.org/10.1088/0953-8984/27/10/102101.
[24] M.V. Fedorov, A.A. Kornyshev, Towards understanding the structure and capacitance of electrical double layer in ionic liquids, Electrochim. Acta 53 (2008) 6835–6840, https://doi.org/10.1016/j.electacta.2008.02.065.
[25] J.K. Ewert, D. Weingarth, C. Denner, M. Friedrich, M. Zeiger, A. Schreiber, R. Kempe, Enhanced capacitance of nitrogen-doped hierarchically porous carbide-derived carbon in matched ionic liquids, J. Mater. Chem. A 3 (2015) 18906–18912, https://doi.org/10.1039/C5TA04773K.
[26] B. Krüner, C. Odenwald, A. Quade, G. Kickelbick, V. Presser, Influence of nitrogen-doping for carbide-derived carbons on the supercapacitor performance in an organic electrolyte and an ionic liquid, Batteries & Supercaps 1 (2018) 135–148, https://doi.org/10.1002/batt.201800051.
[27] F. Lai, J. Feng, R. Yan, G.C. Wang, M. Antonietti, M. Oschatz, Breaking the limits of ionic liquid-based supercapacitors: mesoporous carbon electrodes functionalized with manganese oxide nanosplotches for dense, stable, and wide-temperature energy storage, Adv Funct Mater 28 (2018) 1801298, https://doi.org/10.1002/adfm.201801298.
[28] M. Liu, Y.L. Wang, K. Schutjajew, L. Chai, M. Oschatz, Ion bridging by carbon dioxide facilitates electrochemical energy storage at charged carbon–ionic–liquid interfaces, Adv Energy Mater 13 (2023) 2300401, https://doi.org/10.1002/aenm.202300401.
[29] X.-L. Dong, S.-Q. Wang, B. He, W.-C. Li, Highly sp2 hybridized and nitrogen, oxygen dual-doped nanoporous carbon network: synthesis and application for ionic liquid supercapacitors, Microporous Mesoporous Mater. 259 (2018) 229–237, https://doi.org/10.1016/j.micromeso.2017.06.011.
[30] S.K. Singh, K. Takeyasu, J. Nakamura, Active sites and mechanism of oxygen reduction reaction electrocatalysis on nitrogen-doped carbon materials, Adv. Mater. 31 (2019) 1804297, https://doi.org/10.1002/adma.201804297.
[31] Z.R. Ismagilov, A.E. Shalagina, O.Y. Podyacheva, A.V. Ischenko, L.S. Kibis, A. I. Boronin, E.N. Tkachev, Structure and electrical conductivity of nitrogen-doped carbon nanofibers, Carbon N Y 47 (2009) 1922–1929, https://doi.org/10.1016/j.carbon.2009.02.034.
[32] Y. Li, et al., Pyridinic nitrogen enriched porous carbon derived from bimetal organic frameworks for high capacity zinc ion hybrid capacitors with remarkable rate capability, J. Energy Chem. 56 (2021) 404–411, https://doi.org/10.1016/j.jechem.2020.08.005.
[33] M. Aetizaz, S. Sarfaraz, K. Ayub, Interaction of imidazolium based ionic liquid electrolytes with carbon nitride electrodes in supercapacitors; a step forward for understanding electrode–electrolyte interaction, J Mol Liq 369 (2023) 120955, https://doi.org/10.1016/j.molliq.2022.120955.
[34] R. Yan, K. Leus, J.P. Hofmann, M. Antonietti, M. Oschatz, Porous nitrogen-doped carbon/carbon nanocomposite electrodes enable sodium ion capacitors with high capacity and rate capability, Nano Energy 67 (2020) 104240, https://doi.org/10.1016/j.nanoen.2019.104240.
[35] I.K. Ilic, M. Oschatz, The functional chameleon of materials chemistry—Combining carbon structures into all-carbon hybrid nanomaterials with intrinsic porosity to overcome the "functionality-conductivity-dilemma" in electrochemical energy storage and electrocatalysis, Small 17 (2021) 2007508, https://doi.org/10.1002/smll.202007508.
[36] B. Jürgens, E. Irran, J. Senker, P. Kroll, H. Müller, W. Schnick, Melem (2, 5, 8-triamino-tri-s-triazine), an important intermediate during condensation of melamine rings to graphitic carbon nitride: synthesis, structure determination by X-ray powder diffractometry, solid-state NMR, and theoretical studies, J. Am. Chem. Soc. 125 (2003) 10288–10300, https://doi.org/10.1021/ja0357689.
[37] A. Thomas, A. Fischer, F. Goettmann, M. Antonietti, J.O. Müller, R. Schlögl, J. M. Carlsson, Graphitic carbon nitride materials: variation of structure and morphology and their use as metal-free catalysts, J Mater Chem 18 (2008) 4893–4908, https://doi.org/10.1039/B800274F.
[38] Q. Shi, R. Zhang, Y. Lv, Y. Deng, A.A. Elzatahrya, D. Zhao, Nitrogen-doped ordered mesoporous carbons based on cyanamide as the dopant for supercapacitor, Carbon N Y 84 (2015) 335–346, https://doi.org/10.1016/j.carbon.2014.12.013.
[39] K. Bartle, D. Perry, S. Wallace, The functionality of nitrogen in coal and derived liquids: an XPS study, Fuel Processing Technology 15 (1987) 351–361, https://doi.org/10.1016/0378-3820(87)90057-9.
[40] M. Oschatz, J.P. Hofmann, T.W. van Deelen, W.S. Lamme, N.A. Krans, E.J. Hensen, K.P. de Jong, Effects of the functionalization of the ordered mesoporous carbon support surface on iron catalysts for the Fischer–Tropsch synthesis of lower olefins, ChemCatChem 9 (2017) 620–628, https://doi.org/10.1002/cctc.201601228.

[41] Q. Qin, T. Heil, M. Antonietti, M. Oschatz, Single-site gold catalysts on hierarchical N-doped porous noble carbon for enhanced electrochemical reduction of nitrogen, Small Methods 2 (2018) 1800202, https://doi.org/10.1002/smtd.201800202.
[42] C.L. Perkins, S.-H. Lee, X. Li, S.E. Asher, T.J. Coutts, Identification of nitrogen chemical states in N-doped ZnO via x-ray photoelectron spectroscopy, J Appl Phys 97 (2005), https://doi.org/10.1063/1.1847728.
[43] R. Bardestani, G.S. Patience, S. Kaliaguine, Experimental methods in chemical engineering: specific surface area and pore size distribution measurements—BET, BJH, and DFT, Can J Chem Eng 97 (2019) 2781–2791, https://doi.org/10.1002/cjce.23632.
[44] B.-A. Mei, O. Munteshari, J. Lau, B. Dunn, L. Pilon, Physical interpretations of Nyquist plots for EDLC electrodes and devices, J. Phys. Chem. C 122 (2018) 194–206, https://doi.org/10.1021/acs.jpcc.7b10582.
[45] C. Lei, F. Markoulidis, Z. Ashitaka, C. Lekakou, Reduction of porous carbon/Al contact resistance for an electric double-layer capacitor (EDLC), Electrochim. Acta 92 (2013) 183–187, https://doi.org/10.1016/j.electacta.2012.12.092.